

1 **Dual roles for LUBAC signaling in thymic epithelial cell development and survival**

2

3 Reema Jain^{1,2, #}, Kelin Zhao^{1,2}, Julie M. Sheridan^{1,2}, Melanie Heinlein^{1,2*}, Fiona Kupresanin^{1^},
4 Waruni Abeysekera^{1,2}, Cathrine Hall^{1,2}, James Rickard^{1,2}, Philippe Bouillet^{1,2}, Henning
5 Walczak^{3,4}, Andreas Strasser^{1,2}, John Silke^{1,2}, Daniel H.D. Gray^{1,2§}

6 ¹Walter and Eliza Hall Institute of Medical Research, Melbourne, VIC, Australia; ²Department
7 of Medical Biology, University of Melbourne, Melbourne, VIC, Australia; ³ Centre for Cell
8 Death, Cancer and Inflammation, UCL Cancer Institute, University College London, London,
9 UK, ⁴ Centre for Biochemistry, University of Cologne, Cologne, Germany

10 # Current address Fred Hutchinson Cancer Research Center, Seattle, Washington, USA.

11 * Current address Department of Molecular Oncology, Genentech, Inc., South San Francisco,
12 CA, USA

13 ^ Current address ANZAC Research Institute, Concord, Australia

14
15 §Correspondence to: dgray@wehi.edu.au

16
17 T: +61 3 9345 2741

18 F: +61 3 9347 0852

19

20 **Short Title: Essential functions for LUBAC in thymic epithelium**

21

22

23 **Abstract**

24 Thymic epithelial cells (TECs) form a unique microenvironment that orchestrates T cell
25 differentiation and immunological tolerance. Despite the importance of TECs for adaptive
26 immunity, there is an incomplete understanding of the signalling networks that support their
27 differentiation and survival. We report that the linear ubiquitin chain assembly complex
28 (LUBAC) is essential for medullary TEC (mTEC) differentiation, cortical TEC survival and
29 prevention of premature thymic atrophy. TEC-specific loss of LUBAC proteins, HOIL-1 or
30 HOIP, severely impaired expansion of the thymic medulla and AIRE-expressing cells.
31 Furthermore, HOIL-1-deficiency caused early thymic atrophy due to Caspase-8/MLKL-
32 dependent apoptosis/necroptosis of cortical TECs. By contrast, deficiency in the LUBAC
33 component, SHARPIN, caused relatively mild defects only in mTECs. These distinct roles for
34 LUBAC components in TECs correlate with their function in linear ubiquitination, NF κ B
35 activation and cell survival. Thus, our findings reveal dual roles for LUBAC signaling in TEC
36 differentiation and survival.

37

38 **Introduction**

39 The differentiation of haematopoietic progenitors into naive T cells in the thymus is governed by
40 thymic epithelial cells (TECs). Specialized TEC subtypes direct distinct quality control processes
41 in thymocyte differentiation. Cortical thymic epithelial cells (cTECs) mediate early events,
42 including T cell lineage commitment, proliferation and positive selection of cells expressing
43 TCRs capable of interacting with self-peptide/MHC complexes (1). By contrast, medullary
44 thymic epithelial cells (mTECs) are important for thymic negative selection and the generation
45 of FOXP3⁺ regulatory T (Treg) cells, thus limiting the risk of autoimmunity (2). Medullary TECs
46 are uniquely adapted for the induction of immunological tolerance because they express
47 thousands of tissue-specific antigens that greatly increase the scope of thymic negative selection.
48 This property is mediated in mTEC subtypes by the transcriptional regulators AIRE and FEZF2
49 (2, 3). These essential functions of TEC in immunity and tolerance have generated considerable
50 interest in the molecular mechanisms of their differentiation and maintenance.

51

52 Members of the tumour necrosis factor (TNF) and TNF receptor (TNFR) superfamilies (i.e. the
53 TNFSF and TNFRSF) and NF- κ B transcription factors are critical for TEC differentiation and
54 the establishment of thymic tolerance (4). Signalling through RANK is required for mTECs
55 during development, whereas signals from other TNFRSF members co-ordinate the maintenance
56 of postnatal mTECs (5, 6). Ligation of the TNFRSF members CD40, RANK and lymphotoxin
57 beta receptor (LT β R) is required for the development of the key tolerogenic mTEC populations,
58 such as AIRE^{pos} and FEZF2^{pos} cells (3, 5, 7-9). Yet, precisely how these signals are integrated to
59 direct TEC fate, function and survival remains poorly understood.

60

61 LUBAC is a component of TNFR1 and CD40 receptor signalling complexes (10, 11) that
62 attaches linear ubiquitin chains to signal transducers and/or regulators of the canonical NF- κ B
63 pathway, including RIPK1, TRADD, NEMO and TNFR1 itself (10, 12, 13). LUBAC is a ~600-
64 kD ubiquitin E3 complex composed of three proteins: SHANK-associated RH domain
65 interacting protein (SIPL1/SHARPIN), C3HC4-type zinc finger containing 1 (RBCK1/HOIL-1)
66 and the catalytic component, ring finger protein 31 (RNF31/HOIP) (10, 12, 14-16). Mutations of
67 these LUBAC components perturb innate and adaptive immune responses (10, 17, 18). Patients
68 with loss-of-function mutations in HOIL-1 or HOIP were found to be T cell deficient and (in one
69 patient) had greatly reduced T-cell receptor excision circles, indicating impaired thymic function
70 (17, 18).

71
72 There is a differential requirement for HOIP, HOIL-1 and SHARPIN for LUBAC function,
73 signal transduction, differentiation and cell death. Deficiency in HOIP or HOIL-1 completely
74 abolishes LUBAC activity, impairs NF- κ B activation and promotes cell death (10, 15, 19-21).
75 By contrast, SHARPIN-deficient cells can carry out diminished linear ubiquitination via HOIL-
76 1/HOIP complexes, attenuated activation of NF- κ B and JNK signaling pathways and are also
77 sensitized to cell death (10, 21-23). Importantly, LUBAC functions in NF- κ B activation and cell
78 survival can be independent (24).

79
80 The *in vivo* consequences of these defects vary according to cell type and developmental context.
81 Complete HOIP- or HOIL-1-deficiency causes embryonic lethality due to TNF-induced vascular
82 defects (21, 25). The loss-of-function SHARPIN mutant mice, *cpdm*, are viable but succumb to
83 severe dermatitis from approximately 6 weeks of age (26, 27), primarily due to sensitization to

84 TNF-induced cell death via apoptosis or necroptosis (10, 21-23). Roles for LUBAC in
85 lymphocyte differentiation, activation and survival (e.g. (20, 28, 29)) have also been reported.
86 Key questions in the field remain how complete or partial loss of LUBAC function impacts
87 various tissues and how these defects influence inflammatory and immune pathology (17, 18).

88
89 Given the importance of TNFRSF signaling in TEC and thymic tolerance (7, 9, 30, 31), we
90 investigated whether LUBAC function was required for TEC development and homeostasis.
91 Conditional ablation of HOIP or HOIL-1 in TEC caused severe thymic atrophy and T cell
92 deficiency. HOIL-1 was required for the development of the thymic medulla in young mice and
93 the maintenance of cTEC in adults. Thymic atrophy and the demise of HOIL-1-deficient TECs
94 was driven in part by caspase-8/MLKL-driven apoptosis/necroptosis; blockade of this process
95 restored cortical and medullary microenvironments and thymic T cell production. Conversely,
96 only mild disruption of the thymic microenvironment was observed in SHARPIN-deficient mice,
97 confined to a defect in immature mTECs that was not related to cell death. These findings
98 identify LUBAC as an essential signaling hub with distinct roles in mTEC development, cTEC
99 survival and thymic function.

100

101 **Results**

102 **LUBAC proteins HOIL-1 and HOIP in TECs are essential to maintain thymic function**

103 We first assessed expression of the three LUBAC components in RNAseq data from TEC
104 subpopulations purified from young adult 8 week-old mice. TEC can be sub-divided into three
105 main populations: cTEC, MHC II^{low} mTEC (termed mTEC^{low}) that contain a mixture of
106 precursors and differentiated cells, and MHC II^{high} mTEC (termed mTEC^{high}) including cycling

107 cells and the AIRE+ subset(30). All three known LUBAC components were transcribed in all
108 TEC subsets, with *Rnf31* (encoding HOIP) relatively lower in mTEC^{high}, while mTEC^{low}
109 expressed the highest levels of *Sip11* (encoding SHARPIN) (**Figure 1A**). To determine the roles
110 of LUBAC components in TECs *in vivo*, we generated mice with *Foxn1*^{Cre}-driven deletion of
111 *Rbck1* or *Rnf31*, hereafter termed *Hoil-1*^{ΔFoxn1} and *Hoip*^{ΔFoxn1}, respectively (20, 21, 25) (specific
112 deletion confirmed in **Figure S1A**). Mice in both of these strains were viable, reproduced
113 normally and had no overt health problems. The role of SHARPIN in TEC development was
114 assessed in the spontaneous loss-of-function mutant *cpdm* mouse strain (*Sh*^{cpdm/cpdm}) (26, 27),
115 prior to the onset of inflammation. We observed a modest reduction in the thymic cellularity of
116 *Sh*^{cpdm/cpdm} mice; however, TEC-specific loss of HOIL-1 or HOIP caused severe thymic atrophy
117 in adult mice (**Figure 1B**).

118
119 We tracked thymocyte differentiation *Hoil-1*^{ΔFoxn1} mice by analyzing CD4 vs. CD8 expression
120 and observed loss in all major stages of T cell differentiation (**Figure 1C, Figure S1B**). Deeper
121 analysis of CD4⁺CD8⁻ double negative (DN) precursor stages revealed a proportional block at the
122 DN3 stage of differentiation and numerical loss in all thymocyte precursor stages in *Hoil-1*^{ΔFoxn1}
123 mice (**Figure S1C**). Thymic Treg cell production in 8-week-old *Hoil-1*^{ΔFoxn1} mice was virtually
124 extinguished in the severely atrophic thymi (**Figure S1D**). These data show that TEC-specific
125 HOIL-1 deletion led to severe thymic hypotrophy and markedly impaired T cell differentiation.

126
127 We then compared the thymic phenotype of young (**Figure 1D**) and young adult *Hoip*^{ΔFoxn1} mice
128 (**Figure S1E-G**) and found that they closely resembled that of *Hoil-1*^{ΔFoxn1} mice, with severe
129 deficiency in all major thymocyte subsets. Thus, HOIP and HOIL-1 are critical in TECs for

130 establishing or maintaining thymic function, consistent with the essential roles of these proteins
131 in LUBAC activity (21).

132

133 The thymic defects in adult *Hoil-1*^{*ΔFoxn1*} mice caused T cell lymphopenia in peripheral lymphoid
134 tissues (**Figure S2A**). Both CD4⁺ and CD8⁺ T cells were diminished and, consistent with the
135 thymic atrophy, naïve CD44^{low} CD62L^{high} populations were particularly affected with
136 homeostatic expansion of CD122⁺ “virtual” memory cells (**Figure 1E, F, Figure S2B, C**).
137 Although the proportions of proliferating Ki67⁺ T cells and FOXP3⁺ Treg cells were increased in
138 8-week-old *Hoil-1*^{*ΔFoxn1*} mice, the overall numbers were largely normal (**Figure S2D, E**). This
139 loss of naïve T cell populations yet maintenance of the virtual memory and regulatory subsets is
140 consistent with the greater reliance on thymic output of the former (32). These defects extended
141 to the TCR repertoire, with alterations in T cells expressing distinct TCRβ chains (**Figure S2F**).

142

143 We then assayed thymus size throughout ontogeny to determine whether HOIL-1 was required in
144 TECs for thymic development or homeostasis. Overall thymic cellularity immediately following
145 birth was normal in *Hoil-1*^{*ΔFoxn1*} mice but by day 3-4 mild thymic hypotrophy was evident
146 (**Figure 1G**). All major thymocyte subsets, including Treg cells, were diminished and DN1 and
147 DN3 precursor populations were reduced in 4-day-old *Hoil-1*^{*ΔFoxn1*} mice (**Figure S3A-C**). T cell
148 lymphopenia was not yet evident in the spleen, although a mild reduction in the proportion of
149 naïve CD4⁺ T cells was detected in 4-day-old *Hoil-1*^{*ΔFoxn1*} mice (**Figure S3D-F**). Thymus size in
150 *Hoil-1*^{*ΔFoxn1*} mice peaked at days 9-10 but then atrophied, with approximately 12-fold lower
151 thymic cellularity at 8 weeks of age compared to controls (**Figure 1G**). These data reveal a
152 differential requirement for LUBAC components in TEC maintenance, with HOIL-1 and HOIP

153 essential for thymic function beyond the perinatal stage and the establishment of a normal naïve
154 T cell pool.

155

156 **TECs require HOIL-1 or HOIP for their homeostasis**

157 We next investigated the role of HOIL-1 or HOIP in TEC homeostasis at key time points. Low
158 numbers of TECs could be recovered from the atrophied thymi of aged-matched 13-week-old
159 *Hoil-1*^{ΔFoxn1} (**Figure 2A**) and *Hoip*^{ΔFoxn1} mice (**Figure 2B**). We analysed the phenotype of those
160 TECs that could be recovered and found very similar profiles in both *Hoil-1*^{ΔFoxn1} or *Hoip*^{ΔFoxn1}
161 mice, with severe loss in the number of mTEC (Ly51⁺UEA-1⁺) (**Figure 2C-F**). Examination of
162 the thymic architecture of 8-week-old *Hoil-1*^{ΔFoxn1} or *Hoip*^{ΔFoxn1} mice revealed extensive
163 disruption of cortical and medullary regions (labelled with anti-keratin-8 versus anti-keratin-
164 5/UEA-1), including the AIRE⁺ compartment, which had almost disappeared (**Figure 2G-L**).
165 The loss of TEC in adult *Hoil-1*^{ΔFoxn1} and *Hoip*^{ΔFoxn1} mice was characterized by large epithelial
166 cell-free areas and prominent ERTR7⁺ fibroblastic remodeling (**Figure 2G-L**). These data
167 indicate that HOIL-1 and HOIP are required for the differentiation and/or homeostasis of all
168 major TEC subpopulations in the adult thymus. The identical impact of TEC-specific HOIL-1- or
169 HOIP-deficiency on the thymus and TEC phenotype is consistent with observations in other
170 tissues and the complete ablation of LUBAC-mediated linear ubiquitination caused by loss of
171 either protein (10, 15, 21).

172

173 We next sought to distinguish whether LUBAC activity was required for TEC differentiation or
174 homeostasis. We assayed TEC composition during the development of *Hoil-1*^{ΔFoxn1} mice and
175 observed a slight reduction in total TEC numbers as early as E15.5 that worsened in 4-day

176 postnatal mice (**Figure 3A**). Flow cytometric analysis was used to quantify the major
177 subpopulations of EpCAM⁺ TECs: cTEC and mTEC, and the mTEC subpopulations mTEC^{high}
178 (Ly51⁻UEA-1⁺MHCII⁺CD80^{high}) and mTEC^{low} (Ly51⁻UEA-1⁺MHCII⁺CD80^{low/-}) cells that
179 become apparent in day 4 mice (**Figure 3B-D**). We found a severe deficit in mTEC in embryonic
180 and neonatal thymi from *Hoil-1*^{ΔFoxn1} mice (**Figure 3B-D**), including the tolerogenic AIRE⁺
181 population (**Figure 3E**). The proportion of Ki67⁺ TECs was increased in E15.5 and day 4 *Hoil-*
182 *1*^{ΔFoxn1} mice, suggesting specific loss of non-proliferating TECs and/or compensatory
183 proliferation of remaining cells (**Figure 3F, G**). Therefore, although TECs from *Hoil-1*^{ΔFoxn1}
184 mice were capable of proliferation and differentiation into the major TEC subpopulations, they
185 were unable to maintain normal numbers. By contrast, relatively normal numbers of cTECs were
186 recovered at these stages (**Figure 3C, D**).

187

188 The thymic architecture of neonatal *Hoil-1*^{ΔFoxn1} mice was also perturbed. Although the
189 distribution of ERTR7⁺ fibroblasts was comparable, medullary regions (labelled with anti-
190 keratin-5, UEA-1 and AIRE) were fewer and smaller in *Hoil-1*^{ΔFoxn1} mice at day 4 (**Figure 3H-**
191 **J**). Consistent with the flow cytometric analysis, a normal network of K8⁺ cTECs was apparent
192 in thymi from neonatal *Hoil-1*^{ΔFoxn1} mice (**Figure 3H**). We conclude that HOIL-1 is not required
193 for mTEC differentiation *per se* but is essential for the expansion and maintenance of all mTEC
194 subpopulations in the perinatal thymus. Furthermore, HOIL-1-mediated signals are not required
195 for the early differentiation and expansion of cTECs yet is required for their maintenance and
196 thymic function later in life (**Figure 1, 2**).

197

198 **HOIL-1 is required to prevent TEC necroptosis to sustain thymic function**

219 To explore how the loss of LUBAC function leads to these outcomes, we performed RNAseq
220 analysis on FACS-purified cTEC and mTEC^{high} from 2-week-old *Hoil-1^{lox/lox}* (control) and *Hoil-*
221 *1^{ΔFoxn1}* mice. We selected this age because: 1) it immediately precedes severe thymic atrophy,
222 therefore the relevant transcriptional changes should be underway, 2) sufficient numbers of TEC
223 could be recovered and 3) the relative expression profiles of the LUBAC components was
224 equivalent to young adult mice (**Figure S4A**). Visualization of the relationships among the
225 populations in a multi-dimensional scaling plot showed: (1) that the 3 biological replicates
226 clustered together closely, indicating low experimental variability, (2) the first dimension
227 distinguished cTEC from mTEC^{hi}, and (3) the second dimension distinguished the transcriptional
228 impact of *Hoil-1*-deficiency (**Figure 4A**). Large transcriptional changes were caused by HOIL
229 loss in cTEC and mTEC^{high}, with ~3,000 and ~5,700 genes reaching the thresholds for statistical
230 significance, although these generally had modest overall expression levels (log expression) or
231 fold-changes (**Figure 4B**). KEGG pathway analyses of differentially expressed genes revealed
232 enrichment in those associated with cell adhesion, ECM interaction and various signaling
233 pathways in cTECs, including several metabolic pathways and cell cycle regulators in mTEC^{hi}
234 (**Figure S4B, C**). Interestingly, we observed enrichment of genes involved in regulation of cell
235 projection organization and morphology among HOIL-1 induced transcripts in cTEC (**Figure S4**
236 **D-F**); processes recently implicated in thymic regeneration from aged-related involution (33).
237
238 LUBAC-dependent cell signaling can be required to prevent aberrant cell death via caspase-8-
239 dependent apoptosis and/or by MLKL-dependent necroptosis, depending on the cell type (20-22,
240 24, 29, 34). Hierarchical clustering of the transcriptional profiles of genes involved in receptor-
241 mediated programmed cell death was visualized using heatmaps (**Figure 4C**). These clearly

222 distinguished TEC subsets from the two genotypes, indicating that substantial differences in this
223 pathway were induced by the loss of HOIL-1 (**Figure 4C**). Among these changes, the
224 upregulation of *Mkl1* and *Casp8* was a distinguishing feature of cTECs and mTEC^{high} cells
225 isolated from 2-week-old *Hoil-1^{ΔFoxn1}* mice. These findings suggest that the loss of HOIL-1 in
226 TECs had sensitized them to MLKL-dependent necroptosis and/or caspase-8-driven apoptosis
227 just prior to the onset of severe thymic atrophy.

228

229 To test whether the TEC defects observed in HOIL-1-deficient mice were caused by the
230 induction of cell death, we generated *Hoil-1^{ΔFoxn1}Casp8^{-/-}Mkl1^{-/-}* mice in which both apoptotic and
231 necroptotic pathways are non-functional (35). We first established that young *Casp8^{-/-}Mkl1^{-/-}*
232 mice had normal TN, DP and SP thymocyte differentiation and splenic T cell homeostasis
233 (**Figure 4D, E, S5**), extending on previous analyses (20, 35) and isolating any phenotypes
234 observed in the compound mutants to changes in the TEC compartment. In striking contrast to
235 the severe thymic atrophy and T cell lymphopenia observed in *Hoil-1^{ΔFoxn1}* mice, *Hoil-1^{ΔFoxn1}*
236 *Casp8^{-/-}Mkl1^{-/-}* mice had normal thymic cellularity and near complete restoration of the
237 peripheral T cell population (**Figure 4D, E**). This finding indicates that the combined loss of
238 Caspase-8 and MLKL prevented the thymic atrophy observed in adult *Hoil-1^{ΔFoxn1}* mice.

239

240 Interestingly, the rescue of thymic function was driven by only partial restoration of the thymic
241 microenvironment. *Hoil-1^{lox/lox}Casp8^{-/-}Mkl1^{-/-}* control mice had a reduction in overall TEC
242 number compared to *Hoil-1^{lox/lox}* control mice due to loss of mTEC (**Figure 4F, G**). TEC number
243 was further decreased in *Hoil-1^{ΔFoxn1}Casp8^{-/-}Mkl1^{-/-}* mice, yet was higher than the atrophied
244 thymus of *Hoil-1^{ΔFoxn1}* mice, suggesting only a portion of TEC were rescued (**Figure 4F**). This

245 rescue was accounted for mainly by increased mTEC, although there was a trend (not
246 statistically significant) towards higher cTEC in *Hoil-1^{ΔFoxn1}Casp8^{-/-}Mkl1^{-/-}* compared to *Hoil-1^{ΔFoxn1}*
247 mice (**Figure 4G, H**). Immunofluorescent staining of thymic sections from 8-week-old
248 *Hoil-1^{ΔFoxn1}Casp8^{-/-}Mkl1^{-/-}* mice confirmed that the rescue of HOIL-1-deficient TEC was partial,
249 demonstrating small, isolated medullary islets composing a reduced area compared to the large,
250 confluent medulla of thymi from control mice (**Figure 4I, J, S5F**). In contrast, a normal,
251 confluent K8⁺ cTEC network and cortical microenvironment was observed (**Figure 4I, J**),
252 contrasting the near complete loss of these cells and regions in *Hoil-1^{ΔFoxn1}* mice (**Figure 2 E, F**).
253 Therefore, caspase-8 and MLKL deficiency restored the cortical microenvironment and thymic
254 lymphopoiesis in *Hoil-1^{ΔFoxn1}* mice, but only partially restored the thymic medulla.

255

256 Collectively, these findings demonstrate that a broad transcriptional program is coordinated in
257 TEC by HOIL-1-mediated signals and that antagonism of TEC necroptosis/apoptosis within this
258 program is a critical mechanism supporting thymic function.

259

260 **SHARPIN is required for normal mTEC^{low} compartment**

261 The severe thymic atrophy observed in *Hoil-1^{ΔFoxn1}* and *Hoip^{ΔFoxn1}* mice prompted us to also
262 explore the function of the third LUBAC component, SHARPIN, in TECs and thymic function.
263 To circumvent potentially confounding effects of the psoriasis-like inflammatory syndrome in
264 these *Sh^{cpdm/cpdm}* mice (26), we analyzed TECs and thymic function in *Sh^{cpdm/cpdm}* mice prior to
265 the development of dermatitis. Consistent with previous data (20), we recovered normal
266 proportions of DP thymocytes in *Sh^{cpdm/cpdm}* mice, indicating that no stress-related atrophy had
267 occurred. Nevertheless, mild thymic hypotrophy was accompanied by a trend towards lower

268 TEC numbers (**Figures 1B and 5A**), with half the normal number of mTEC^{low} in *Sh^{cpdm/cpdm}* mice
269 (**Figure 5B, C**). The numbers of cTEC, mTEC^{high}, AIRE⁺ TECs and the proportions of
270 proliferating Ki67⁺ TECs were similar in controls and *Sh^{cpdm/cpdm}* mice (**Figure 5C, S6A, S6B**).
271 The observed mTEC^{low} defect was not recapitulated in *Sh^{cpdm/cpdm} → wt* (Ly5.1) hematopoietic
272 chimeras (**Figure S6C-F**), indicating that the mTEC^{low} defect was a primary consequence of the
273 loss of SHARPIN in the thymic stroma. Analysis of the thymic architecture of *Sharpin^{cpdm/cpdm}*
274 mice revealed mild disruption of the thymic medulla compared to controls, although the location
275 and frequency of AIRE⁺ TECs and ERTR7⁺ fibroblasts were comparable to controls (**Figure 5D-**
276 **F**). We conclude that SHARPIN-mediated signals are required specifically to maintain the
277 mTEC^{low} population.

278

279 SHARPIN is required to antagonize TNF-induced cell death in certain contexts (10). This pro-
280 survival activity is not dependent on NF-κB signaling but involves direct linear ubiquitination of
281 the TNFR1 signalling complex, recruitment of IKK complexes to phosphorylate RIPK1 and
282 prevent caspase-8-mediated apoptosis or RIPK3/MLKL-dependent necroptosis (10, 22-24). To
283 test whether the loss of mTEC^{low} in *Sh^{cpdm/cpdm}* mice was driven by TNF-induced, caspase-8-
284 dependent apoptosis or RIPK3- and MLKL-dependent necroptosis, we assayed for rescue of the
285 phenotype when these pathways were disabled. Genetic ablation of both caspase-8-driven
286 apoptosis and RIPK3/MLKL-dependent necroptosis in *Sh^{cpdm/cpdm} Casp8^{+/-} Ripk3^{-/-}* and
287 *Sh^{cpdm/cpdm} Casp8^{-/-} Mkl^{-/-}* mice failed to rescue the loss of mTEC^{low} observed in *Sh^{cpdm/cpdm}* mice
288 (**Figure 5G**). Consistent with this finding, *Sh^{cpdm/cpdm} Tnf^{-/-}* mice also exhibited the loss of
289 mTEC^{low} (**Figure 5H**). These data indicate that cell death driven by TNF or other death ligands
290 was not the cause of the mTEC defect in *Sh^{cpdm/cpdm}* mice. Therefore, we conclude that LUBAC

291 deprived of SHARPIN sustains sufficient activity to support TEC survival and thymic function
292 but cannot maintain a normal mTEC^{low} population.

293

294 **Discussion**

295 The attachment of Met1-linked “linear” chains of ubiquitin to proteins has emerged as a key
296 regulator of NF- κ B and cell death signaling in inflammation, cell survival and differentiation
297 (36). LUBAC is the only E3 ligase complex known to mediate this form of ubiquitination and it
298 is composed of SHARPIN, HOIL-1 and HOIP. The loss of HOIP or HOIL-1 completely
299 abolishes linear ubiquitination. SHARPIN deficiency only partially reduces this activity, with
300 residual HOIL-1/HOIP complexes sufficient to sustain some LUBAC function in NF- κ B-related
301 programs and the prevention of cell death induced by death ligands other than TNF (10, 12, 14,
302 21, 22, 25, 34). Given the critical roles of TNFR family members and NF- κ B signaling in mTEC
303 differentiation and homeostasis (4), we tested the importance of LUBAC function in TECs. Our
304 data highlight essential roles for LUBAC signalling in mTEC development on one hand, and
305 cTEC survival in adulthood on the other.

306

307 Conditional ablation of either HOIL-1 or HOIP in TECs greatly diminished all mTEC subsets
308 and the formation of the medulla early in life. This phenotype resembles that observed in mice
309 with compound deficiency in the TNFRSF members RANK plus CD40 or LT β R plus CD40 (7,
310 9, 37), or those with loss of the NF- κ B signaling proteins NIK, TRAF6 or REL-B, where severe
311 loss of multiple mTEC subpopulations was observed (4). It is likely that the requirement for the
312 LUBAC for optimal NF- κ B signaling explains the mTEC defects observed in HOIL-1-deficient
313 mice. However, we also found that *Hoil-1* ^{Δ Foxn1} mice succumbed to premature thymic atrophy
314 associated with loss of cTEC in adult animals, which appears to be a novel phenotype. These
315 cTEC defects are highly likely to cause the collapse of thymic function, since most thymocyte
316 proliferation is driven by this microenvironment. It is possible that LUBAC signals may be

317 required for an aspect of cTEC function critical to the production of DP thymocytes, the loss of
318 which then feeds back to cause more severe defects in this compartment. Although Shen *et al.*
319 reported loss of cTEC in young *Nik^{ΔFoxn1}* mice, this phenotype was likely a secondary
320 consequence of the severe autoimmune hepatitis and pneumonitis in these mice, resulting in the
321 stress-induced loss of DP thymocytes (38) required to support this thymic microenvironment. By
322 contrast, *Hoil-1^{ΔFoxn1}* and *Hoip^{ΔFoxn1}* mice were overtly healthy and had no signs of stress-
323 induced DP thymocyte death.

324

325 The spontaneous upregulation of genes involved in apoptosis and necroptosis in HOIL-1-
326 deficient TEC hinted that the induction of aberrant cell death might drive their loss; a notion
327 supported by the rescue of the thymic cortex and thymic function in *Hoil-1^{ΔFoxn1}Casp8^{-/-}Mkl1^{-/-}*
328 mice. This finding is in accord with observations that LUBAC-deficiency in certain cell types
329 can predispose them to TNF-induced apoptosis (which is caspase-8-dependent) or necroptosis
330 (which is RIPK1/RIPK3/MLKL-dependent)(10, 21, 22, 25, 39). Although our genetic data
331 implicate aberrant cell death in the TEC loss, cortical collapse and thymic atrophy observed in
332 *Hoil-1^{ΔFoxn1}* mice, only a modest increase in overall TEC number was observed in *Hoil-*
333 *1^{ΔFoxn1}Casp8^{-/-}Mkl1^{-/-}* mice, despite restoration of a normal, confluent K8⁺ cTEC network. This
334 observation may reflect a technical limitation of flow cytometric analysis of TEC, whereby the
335 recovery of cTEC greatly underestimates the total number of these cells, as established by
336 Sakata, *et al.* (40). Other approaches will be required to confirm whether loss of LUBAC
337 function primarily impacts cTEC survival *in vivo*. Alternatively (or in addition), defective
338 regulation of cTEC morphology may influence the atrophy observed in *Hoil-1^{ΔFoxn1}* mice. We
339 found changes in the expression of genes regulating cellular projections in cTEC from *Hoil-*

340 *I^{ΔFoxn1}* mice, reminiscent of features reported in thymic regeneration in aged mice that were
341 independent of cTEC numerical changes(33). While the precise mechanisms remain to be
342 determined, it is clear that the main lymphopoietic cTEC niches were restored in *Hoil-*
343 *I^{ΔFoxn1}Casp8^{-/-}Mkl^{-/-}* mice, uncovering a critical signaling axis in the cTEC essential for thymic
344 function.

345

346 We also found that the restoration of the medulla was not complete in *Hoil-I^{ΔFoxn1}Casp8^{-/-}Mkl^{-/-}*
347 mice, therefore it is likely LUBAC modulates other signals supporting TEC expansion and/or
348 survival. In this regard, we note our RNAseq analysis of TEC from *Hoil-I^{ΔFoxn1}* mice revealed
349 heightened transcription of *Trp53* which, although required for TEC function (41), can also
350 activate cell death and senescence (42). Future studies will reveal how LUBAC activity
351 intersects with these pathways to impact TEC differentiation, survival and function.

352

353 Consistent with the subordinate role for SHARPIN in linear ubiquitination, thymi from
354 *Sh^{cpdm/cpdm}* mice exhibited milder TEC defects. Although there was a reduction in mTEC^{low} in
355 *Sh^{cpdm/cpdm}* mice compared to controls, all other major TEC subsets were normal. Thus, there
356 appears to be sufficient LUBAC activity in SHARPIN-deficient TEC to support near normal
357 thymic function and homeostasis. Since compound loss of TNF or Caspase-8 plus RIPK3 or
358 Caspase-8 and MLKL did not restore the mTEC^{low} compartment of *Sh^{cpdm/cpdm}* mice, we conclude
359 that the reduced LUBAC activity in *Sh^{cpdm/cpdm}* mice did not predispose these TECs to cell death.
360 Rather, it is likely that SHARPIN is required for the optimal transduction of NF-κB signaling,
361 perhaps downstream of CD40/CD40L interactions, which have previously been shown to
362 mediate mTEC^{low} survival and/or expansion (7, 30).

363

364 In conclusion, this study defines differential roles for LUBAC components in TECs that correlate
365 with their function in linear ubiquitination. These data reveal dual roles for LUBAC in the
366 development and maintenance of the thymic microenvironment.

367 **Methods**

368 **Mice**

369 The *Sharpin*^{cpdm/cpdm} mutant mouse strain arose on a C57BL/6/Ka background (26) and these
370 mice were backcrossed twice onto a C57BL/6 background (22). The *Foxn1*^{cre}, *Rnf31*^{lox}, *Rbck1*^{lox},
371 *Sh*^{cpdm/cpdm}*TNF*^{-/-}, *Sh*^{cpdm/cpdm}*Casp8*^{-/-}*Mkl1*^{-/-} and *Sh*^{cpdm/cpdm}*Casp8*^{+/-}*Ripk3*^{-/-} were generated as
372 previously described (20, 22, 25, 43) and were maintained on a C57BL/6 background. No
373 randomisation or blinding of animals was performed for experiments. All mice were housed
374 under specific pathogen-free housing conditions according to the regulations of the Walter and
375 Eliza Hall Institute of Medical Research.

376

377 **Thymus digestion**

378 This procedure is described in detail elsewhere (44); briefly, the two thymic lobes were separated
379 and connective tissue was removed with forceps. Snips were made in each lobe with surgical
380 scissors and the fragments were agitated in 5 mL of RPMI-1640 medium with 25.96 mM HEPES
381 with a wide-bore pipette tip. The supernatant was recovered and replaced by 1 mL of digestion
382 buffer (RPMI-HEPES supplemented with 0.5 Wunsch units Liberase TM (Roche) and DNase I
383 at 0.1% (w/v) (Sigma-Aldrich)). Thymic tissue was then digested at 37°C for 15 min with gentle
384 agitation after every 5 min. The supernatant was then replaced with 500 µL of digestion buffer
385 and the digestion incubation was repeated for 15 min. The single cell suspensions recovered as
386 Fractions 1 and 2 were stained with antibodies to analyze TEC phenotype and number.

387

388 **Flow cytometry**

389 Single-cell suspensions of lymphoid tissue were stained with various fluorochrome-conjugated
390 antibodies. Surface staining of TECs was performed using the following antibodies that were
391 made at The Walter and Eliza Hall Institute, unless otherwise stated. The TEC lineage depletion
392 cocktail consisted of antibodies against mouse CD16/32 (FcγR-block, clone 2.4G2), mouse
393 CD45 PerCP/Cy5.5 (clone 30-F11, Biolegend), mouse CD31 PerCP/Cy5.5 (clone 390,
394 Biolegend) and mouse TER119 PerCP/Cy5.5 (clone TER119, Biolegend). Other conjugates
395 included antibodies to mouse CD326 (EpCAM) APC/Cy7 (clone G8.8, Biolegend), H2-A/E
396 FITC or APC (clone M5/114.15.2), H2-A/E BV421 (clone M5/114.15.2, Biolegend),
397 biotinylated UEA-1 lectin (Vector labs, USA), mouse Ly51 PE or FITC (clone 6C3, Biolegend)
398 and CD80 BV421 (clone 16-10A1, Biolegend). Second step staining with streptavidin PE/Cy7
399 (BD Biosciences, USA) was used to detect biotinylated UEA1 (Vector Laboratories). Propidium
400 iodide (PI) or DAPI at a final concentration of 2.5 µg/mL was added to unfixed samples just
401 prior to data acquisition to label dead cells. Intracellular staining with antibodies against human
402 Ki67 FITC (clone MOPC-21, BD Pharmingen) and mouse AIRE FITC (clone 5H12) was
403 performed after fixation and permeabilization using the FoxP3 detection kit (eBioscience).
404 Lymphocytes were stained using antibodies of the following specificities: mouse TCRβ PE/Cy7
405 (H57.59.1, Biolegend), mouse CD4 APC (clone H129), mouse CD4 PerCP/Cy5.5 (GK1.5,
406 Biolegend), mouse CD8 APC/Cy7 or BV650 (clone 53-6.7, Biolegend), mouse CD25 PE or
407 BV510 (clone PC61, Biolegend), mouse CD44 PE or FITC (clone IM781), mouse CD122 PE
408 (clone TM-β1), mouse CD62L APC/Cy7 (clone MEL-14, Biolegend) and mouse FOXP3 eFluor-
409 450 (clone FJK-165, eBioscience). The immature thymocyte depletion cocktail contained
410 biotinylated antibodies against mouse NK1.1 (clone PK136, Biolegend), TER119 (TER119),
411 GR1 (clone RB6-8C5), Mac-1 (clone M1-170) and B220 (RA3-6B2), and they were detected

412 with streptavidin BV786 (Biolegend). Screening of TCRV β repertoire in the CD4⁺ and CD8⁺
413 populations was performed with the mouse V β TCR Screening Panel (BD Pharmingen). Samples
414 were acquired using Fortessa X20 (BD Biosciences) and LSR II analysers (BD Bioscience) and
415 data analyzed using FlowJo software 9.9 (TreeStar).

416 **PCR**

417 The floxed allele (in the absence of Cre) in sorted TECs (CD45⁻MHCII⁺EpCAM⁺), stromal cells
418 (CD45⁻EpCAM⁻) and hematopoietic cells (CD45⁺EpCAM⁻) from 3-4 week-old *Hoil-1^{lox/lox}* and
419 *Hoil-1 ^{Δ Foxn1}* mice was detected by using *Hoil-1*-Fwd 5'-ACC CTA GGC CTA GTC AGT GCA
420 AA-3' with *Hoil-1*-Rev-5'-AGG CTG TGG TCC ATT CTA GCC AT-3' producing 580bp band.
421 The conditions were: 96 °C 2 min; 30 cycles for 96 °C 20 s, 57 °C 20 s, 72 °C 1 min 20 s and
422 final extension of 72 °C 5 min. The deleted allele (after Cre-mediated recombination) was
423 detected by using Fwd 5'- ATG GTC TAC AGA AGA AAA CAG GC-3' and Rev 5'-GGG
424 AGA TTC AGA CAA GGT TTC-3' producing 581bp. The conditions were: 94°C 4 min; 30
425 cycles for 94°C 40 s, 55°C 30 s, 72°C 1 min and final extension of 72°C 5 min.

426

427 **Immunohistology**

428 Thymi from adult (8 weeks) and neonatal (day 4) mice were isolated, embedded in Tissue-Tek
429 O.C.T compound (Sakura Finetek, U.S.A.) and snap frozen in a liquid nitrogen/isopentane
430 slurry. Sections of 5-8 μ m were cut using a Microm HM550 Cryostat (Thermo Scientific).
431 Sections were fixed in ice cold acetone (Merck) for 3 min and air-dried for 2 min. Sections were
432 blocked with 5% (v/v) goat serum in PBS with 0.1% Tween-20 (v/v) for 30 min at room
433 temperature before incubation with primary antibodies for 30 min. Primary antibodies of the
434 following specificities were used: mouse K5 (Covance, clone Poly 19055), biotinylated mouse

435 pan-keratin (LifeSpan BioSciences, clone Lu-5), biotinylated UEA-1 lectin (Vector labs, USA),
436 mouse AIRE-Alexa647 (clone 5H12), mouse K8 (clone Troma-I, DSHB) and ER-TR7 (provided
437 by Prof Richard Boyd, Monash University). Following three 5 min washes in PBS, sections were
438 incubated with appropriate secondary reagents (antibodies or streptavidin) conjugated to
439 fluorochromes (anti-rabbit IgG Alexa-555 (Life Technologies) and streptavidin FITC
440 (Invitrogen)) for 30 min, counterstained with DAPI (Sigma-Aldrich), then mounted with
441 Vectashield (Vector labs). Images were collected using a LSM780 confocal microscope with Zen
442 2012 SP2 (black) software v11.0 (Zeiss). Single optical sections and maximal intensity
443 projection images were processed for presentation using OMERO (45) or ImageJ (2.0.0). For
444 quantification of medullary area, 1 of 40 neighbouring sections, or every 1 of 20 for thymic from
445 adult *Hoil-1^{ΔFoxn1}* mice, were selected as a representative section, stained with UEA-1(40) and
446 processed using ImageJ (2.0.0).

447

448 **RNA sequencing**

449 Thymi were pooled from 8- or 2-week-old WT mice and digested to isolate TECs (CD45⁻
450 MHCII⁺EpCAM⁺) (44). At the end of the digestion, fractions were pooled, enriched and purified
451 using anti-mouse CD45 microbeads (Miltenyi Biotec, Germany, Cat # 130052301) and FACS
452 ARIA (BD). Cell pellets were snap frozen on dry ice and stored at -80°C. RNA was isolated
453 using the miRNeasy Micro Kit (Qiagen) with on column DNase digestion according to
454 manufacturer's instructions. First strand cDNA synthesis and cDNA amplification were
455 performed using the SMART-Seq® v4 Ultra® Low Input RNA Kit for Sequencing (Clontech
456 Laboratories) according to manufacturer's instructions. Complementary DNA (cDNA) libraries
457 were prepared and indexed separately using the Nextera® XT DNA Library Preparation Kit

458 (Illumina) following manufacturer's instructions. Each indexed cDNA sample library was
459 quantified using the Agilent TAPE station and the Qubit™ DNA BR assay kit for Qubit 3.0®
460 Fluorometer (Life technologies). The indexed sample libraries were pooled and diluted to 1.5pM
461 for 75 base paired-end sequencing on a NextSeq 500 instrument using the v2 150 cycle High
462 Output kit (Illumina) according to the manufacturer's instructions.

463 Between 13 and 35 million read pairs were generated for each sample and reads were aligned to
464 the *Mus musculus* genome (mm10) using Rsubread (46). The number of read pairs overlapping
465 mouse Entrez genes was summarized using featureCounts and Rsubread's built-in NCBI gene
466 annotation. Low expressed genes were filtered out using edgeR's filterByExpr function (47).
467 Genes without current annotation were also filtered. Differential expression (DE) analyses were
468 undertaken using the edgeR and limma (48) software packages. Library sizes were normalized
469 using the trimmed mean of M-values (TMM) method (49). Sample quality weights were
470 estimated using voomWithQualityWeights (50) and differential expression was evaluated using
471 voom (51) with robust empirical Bayes estimation of the variances (52). Correlations between
472 repeated measurements from the same mouse were estimated using the duplicateCorrelation
473 method (53). The false discovery rate (FDR) was controlled below 0.05 using the method of
474 Benjamini and Hochberg. Over-representation of Gene Ontology (GO) terms and KEGG
475 pathways for the differentially expressed genes were identified using limma's goana and kegg
476 functions. Barcode plots illustrating the cross correlations between the cell types, and enrichment
477 of interested pathway genes were drawn using limma's barcodeplot function. Gene set
478 enrichment tests used the roast method (54). Heatmaps were drawn using limma's coolmap
479 function. Sequence data that support the findings of this study have been deposited with GEO
480 with the primary accession code GSE139898.

481

482 **Hematopoietic reconstitution experiments**

483 Bone marrow reconstitution experiments were performed using recipient WT (C57BL/6-Ly5.1)
484 mice irradiated with 2x 550 RAD and reconstituted within 24 hours by intravenous injection with
485 5×10^6 of BM cells from donors of interest (all on a C57BL/6-Ly5.2 background). Reconstituted
486 mice were analyzed 6.5 weeks after reconstitution.

487

488 **Data analysis**

489 Statistical analyses were performed using Prism version 7. Experiments containing three or more
490 groups were analyzed using ANOVA followed by a Tukey's post-hoc test. Experiments with two
491 groups were analyzed with two-tailed Student's t-test. P-values <0.05 were considered as the
492 threshold for statistical significance for all statistical tests.

493

494 **Author contributions**

495 Conceptualization, R.J., A.S. and D.H.D.G.; Methodology, R.J., J.M.S., K.Z., A.S. and
496 D.H.D.G.; Investigation, R.J., J.M.S., M.H., W.A., K.Z., F.K. and D.H.D.G.; Resources, P.B.,
497 C.H., J.R., H.W., J.S., A.S., D.H.D.G.; Writing - Original draft, R.J., J.M.S., and D.H.D.G.;
498 Writing – Review and editing, R.J., J.M.S., M.H., K.Z., A.S., H.W., J.S. and D.H.D.G. The
499 authors declare no conflict of interest. Correspondence and requests for materials should be
500 addressed to D.H.D.G. (dgray@wehi.edu.au).

501

502 **Acknowledgments**

503 We gratefully acknowledge the Gray, Strasser and Herold laboratories and Dr Nieves Peltzer for
504 valuable feedback on this study. We thank the WEHI Flow Cytometry Laboratory and the Centre
505 for Dynamic Imaging; B Helbert, K Mackwell, C Young for mouse genotyping; G Siciliano, H
506 Marks, K Humphreys and S O'Connor for animal husbandry; and L Tai for technical assistance.
507 TROMA-I was deposited to the DSHB by Brulet, P./Kemler, R. (DSHB Hybridoma Product
508 TROMA-I). This work was supported by grants GNT0637353, GNT1049724, GNT1187367,
509 GNT1025594 and GNT1121325 and Fellowships 1090236 and 1158024 (for D.H.D.G.),
510 Principle Research Fellowship 1016701 (for J.S.), Senior Principal Research Fellowship
511 1020363 (for A.S) from the Australian National Health and Medical Research Council and the
512 Leukaemia Research Foundation. R.J. was supported by MIRS and MIFRS from the University
513 of Melbourne. H.W. is supported by an Alexander von Humboldt Professorship Award, a
514 Wellcome Trust Investigator Award (214342/Z/18/Z), a Cancer Research UK programme grant
515 (A27323), a Medical Research Council UK Grant (MR/S00811X/1) and by the German
516 Research Foundation (DFG) in the context of SFB 1399 and SFB 1403. This work was made
517 possible through Victorian State Government Operational Infrastructure Support and Australian
518 Government NHMRC IRIISS. The authors have no conflicting financial interests.

519

520 **Conflicts of Interest Statement**

521 The authors declare no competing conflicts of interest.

522 **References**

- 523 1. Petrie HT, Zuniga-Pflucker JC. Zoned out: functional mapping of stromal signaling
524 microenvironments in the thymus. *Annu Rev Immunol.* 2007;25:649-79.
- 525 2. Klein L, Kyewski B, Allen PM, Hogquist KA. Positive and negative selection of the T
526 cell repertoire: what thymocytes see (and don't see). *Nat Rev Immunol.* 2014;14(6):377-91.
- 527 3. Takaba H, Morishita Y, Tomofuji Y, Danks L, Nitta T, Komatsu N, et al. Fezf2
528 Orchestrates a Thymic Program of Self-Antigen Expression for Immune Tolerance. *Cell.*
529 2015;163(4):975-87.
- 530 4. Abramson J, Anderson G. Thymic Epithelial Cells. *Annu Rev Immunol.* 2017;35:85-118.
- 531 5. Cosway EJ, Lucas B, James KD, Parnell SM, Carvalho-Gaspar M, White AJ, et al.
532 Redefining thymus medulla specialization for central tolerance. *J Exp Med.* 2017.
- 533 6. Sun SC. The non-canonical NF-kappaB pathway in immunity and inflammation. *Nat Rev*
534 *Immunol.* 2017.
- 535 7. Akiyama T, Shimo Y, Yanai H, Qin J, Ohshima D, Maruyama Y, et al. The tumor
536 necrosis factor family receptors RANK and CD40 cooperatively establish the thymic medullary
537 microenvironment and self-tolerance. *Immunity.* 2008;29(3):423-37.
- 538 8. Desanti GE, Cowan JE, Baik S, Parnell SM, White AJ, Penninger JM, et al.
539 Developmentally regulated availability of RANKL and CD40 ligand reveals distinct mechanisms
540 of fetal and adult cross-talk in the thymus medulla. *J Immunol.* 2012;189(12):5519-26.
- 541 9. Hikosaka Y, Nitta T, Ohigashi I, Yano K, Ishimaru N, Hayashi Y, et al. The cytokine
542 RANKL produced by positively selected thymocytes fosters medullary thymic epithelial cells
543 that express autoimmune regulator. *Immunity.* 2008;29(3):438-50.

- 544 10. Gerlach B, Cordier SM, Schmukle AC, Emmerich CH, Rieser E, Haas TL, et al. Linear
545 ubiquitination prevents inflammation and regulates immune signalling. *Nature*.
546 2011;471(7340):591-6.
- 547 11. Haas TL, Emmerich CH, Gerlach B, Schmukle AC, Cordier SM, Rieser E, et al.
548 Recruitment of the linear ubiquitin chain assembly complex stabilizes the TNF-R1 signaling
549 complex and is required for TNF-mediated gene induction. *Mol Cell*. 2009;36(5):831-44.
- 550 12. Tokunaga F, Nakagawa T, Nakahara M, Saeki Y, Taniguchi M, Sakata S, et al.
551 SHARPIN is a component of the NF-kappaB-activating linear ubiquitin chain assembly
552 complex. *Nature*. 2011;471(7340):633-6.
- 553 13. Draber P, Kupka S, Reichert M, Draberova H, Lafont E, de Miguel D, et al. LUBAC-
554 Recruited CYLD and A20 Regulate Gene Activation and Cell Death by Exerting Opposing
555 Effects on Linear Ubiquitin in Signaling Complexes. *Cell Rep*. 2015;13(10):2258-72.
- 556 14. Ikeda F, Deribe YL, Skanland SS, Stieglitz B, Grabbe C, Franz-Wachtel M, et al.
557 SHARPIN forms a linear ubiquitin ligase complex regulating NF-kappaB activity and apoptosis.
558 *Nature*. 2011;471(7340):637-41.
- 559 15. Kirisako T, Kamei K, Murata S, Kato M, Fukumoto H, Kanie M, et al. A ubiquitin ligase
560 complex assembles linear polyubiquitin chains. *EMBO J*. 2006;25(20):4877-87.
- 561 16. Yamanaka K, Ishikawa H, Megumi Y, Tokunaga F, Kanie M, Rouault TA, et al.
562 Identification of the ubiquitin-protein ligase that recognizes oxidized IRP2. *Nat Cell Biol*.
563 2003;5(4):336-40.
- 564 17. Boisson B, Laplantine E, Dobbs K, Cobat A, Tarantino N, Hazen M, et al. Human HOIP
565 and LUBAC deficiency underlies autoinflammation, immunodeficiency, amylopectinosis, and
566 lymphangiectasia. *J Exp Med*. 2015;212(6):939-51.

- 567 18. Boisson B, Laplantine E, Prando C, Giliani S, Israelsson E, Xu Z, et al.
568 Immunodeficiency, autoinflammation and amylopectinosis in humans with inherited HOIL-1 and
569 LUBAC deficiency. *Nat Immunol.* 2012;13(12):1178-86.
- 570 19. Liang Y, Seymour RE, Sundberg JP. Inhibition of NF-kappaB signaling retards
571 eosinophilic dermatitis in SHARPIN-deficient mice. *J Invest Dermatol.* 2011;131(1):141-9.
- 572 20. Teh CE, Lalaoui N, Jain R, Policheni AN, Heinlein M, Alvarez-Diaz S, et al. Linear
573 ubiquitin chain assembly complex coordinates late thymic T-cell differentiation and regulatory
574 T-cell homeostasis. *Nat Commun.* 2016;7:13353.
- 575 21. Peltzer N, Darding M, Montinaro A, Draber P, Draberova H, Kupka S, et al. LUBAC is
576 essential for embryogenesis by preventing cell death and enabling haematopoiesis. *Nature.*
577 2018;557(7703):112-7.
- 578 22. Rickard JA, Anderton H, Etemadi N, Nachbur U, Darding M, Peltzer N, et al. TNFR1-
579 dependent cell death drives inflammation in Sharpin-deficient mice. *Elife.* 2014;3.
- 580 23. Kumari S, Redouane Y, Lopez-Mosqueda J, Shiraishi R, Romanowska M, Lutzmayer S,
581 et al. Sharpin prevents skin inflammation by inhibiting TNFR1-induced keratinocyte apoptosis.
582 *Elife.* 2014;3.
- 583 24. Lafont E, Draber P, Rieser E, Reichert M, Kupka S, de Miguel D, et al. TBK1 and
584 IKKepsilon prevent TNF-induced cell death by RIPK1 phosphorylation. *Nat Cell Biol.*
585 2018;20(12):1389-99.
- 586 25. Peltzer N, Rieser E, Taraborrelli L, Draber P, Darding M, Pernaute B, et al. HOIP
587 deficiency causes embryonic lethality by aberrant TNFR1-mediated endothelial cell death. *Cell*
588 *Rep.* 2014;9(1):153-65.

- 589 26. HogenEsch H, Gijbels MJ, Offerman E, van Hooft J, van Bekkum DW, Zurcher C. A
590 spontaneous mutation characterized by chronic proliferative dermatitis in C57BL mice. *Am J*
591 *Pathol.* 1993;143(3):972-82.
- 592 27. Seymour RE, Hasham MG, Cox GA, Shultz LD, Hogenesch H, Roopenian DC, et al.
593 Spontaneous mutations in the mouse Sharpin gene result in multiorgan inflammation, immune
594 system dysregulation and dermatitis. *Genes Immun.* 2007;8(5):416-21.
- 595 28. Park Y, Jin HS, Lopez J, Lee J, Liao L, Elly C, et al. SHARPIN controls regulatory T
596 cells by negatively modulating the T cell antigen receptor complex. *Nat Immunol.*
597 2016;17(3):286-96.
- 598 29. Webb LV, Barbarulo A, Huysentruyt J, Vanden Berghe T, Takahashi N, Ley S, et al.
599 Survival of Single Positive Thymocytes Depends upon Developmental Control of RIPK1 Kinase
600 Signaling by the IKK Complex Independent of NF-kappaB. *Immunity.* 2019;50(2):348-61 e4.
- 601 30. Gray DH, Seach N, Ueno T, Milton MK, Liston A, Lew AM, et al. Developmental
602 kinetics, turnover, and stimulatory capacity of thymic epithelial cells. *Blood.* 2006;108(12):3777-
603 85.
- 604 31. Williams JA, Zhang J, Jeon H, Nitta T, Ohigashi I, Klug D, et al. Thymic medullary
605 epithelium and thymocyte self-tolerance require cooperation between CD28-CD80/86 and
606 CD40-CD40L costimulatory pathways. *J Immunol.* 2014;192(2):630-40.
- 607 32. den Braber I, Mugwagwa T, Vrisekoop N, Westera L, Mogling R, de Boer AB, et al.
608 Maintenance of peripheral naive T cells is sustained by thymus output in mice but not humans.
609 *Immunity.* 2012;36(2):288-97.

- 610 33. Venables T, Griffith AV, DeAraujo A, Petrie HT. Dynamic changes in epithelial cell
611 morphology control thymic organ size during atrophy and regeneration. *Nat Commun.*
612 2019;10(1):4402.
- 613 34. Taraborrelli L, Peltzer N, Montinaro A, Kupka S, Rieser E, Hartwig T, et al. LUBAC
614 prevents lethal dermatitis by inhibiting cell death induced by TNF, TRAIL and CD95L. *Nat*
615 *Commun.* 2018;9(1):3910.
- 616 35. Alvarez-Diaz S, Dillon CP, Lalaoui N, Tanzer MC, Rodriguez DA, Lin A, et al. The
617 Pseudokinase MLKL and the Kinase RIPK3 Have Distinct Roles in Autoimmune Disease
618 Caused by Loss of Death-Receptor-Induced Apoptosis. *Immunity.* 2016;45(3):513-26.
- 619 36. Peltzer N, Walczak H. Cell Death and Inflammation - A Vital but Dangerous Liaison.
620 *Trends Immunol.* 2019;40(5):387-402.
- 621 37. Jenkinson SR, Williams JA, Jeon H, Zhang J, Nitta T, Ohigashi I, et al. TRAF3 enforces
622 the requirement for T cell cross-talk in thymic medullary epithelial development. *Proc Natl Acad*
623 *Sci U S A.* 2013;110(52):21107-12.
- 624 38. Shen H, Ji Y, Xiong Y, Kim H, Zhong X, Jin MG, et al. Medullary thymic epithelial NF-
625 kB-inducing kinase (NIK)/IKKalpha pathway shapes autoimmunity and liver and lung
626 homeostasis in mice. *Proc Natl Acad Sci U S A.* 2019;116(38):19090-7.
- 627 39. Shimizu Y, Taraborrelli L, Walczak H. Linear ubiquitination in immunity. *Immunol Rev.*
628 2015;266(1):190-207.
- 629 40. Sakata M, Ohigashi I, Takahama Y. Cellularity of Thymic Epithelial Cells in the
630 Postnatal Mouse. *J Immunol.* 2018;200(4):1382-8.

631 41. Rodrigues PM, Ribeiro AR, Perrod C, Landry JJM, Araujo L, Pereira-Castro I, et al.
632 Thymic epithelial cells require p53 to support their long-term function in thymopoiesis in mice.
633 Blood. 2017;130(4):478-88.

634 42. Aubrey BJ, Kelly GL, Janic A, Herold MJ, Strasser A. How does p53 induce apoptosis
635 and how does this relate to p53-mediated tumour suppression? Cell Death Differ.
636 2018;25(1):104-13.

637 43. Zuklys S, Gill J, Keller MP, Hauri-Hohl M, Zhanybekova S, Balciunaite G, et al.
638 Stabilized beta-catenin in thymic epithelial cells blocks thymus development and function. J
639 Immunol. 2009;182(5):2997-3007.

640 44. Jain R, Gray DH. Isolation of thymic epithelial cells and analysis by flow cytometry.
641 Curr Protoc Immunol. 2014;107:3 26 1-15.

642 45. Allan C, Burel JM, Moore J, Blackburn C, Linkert M, Loynton S, et al. OMERO:
643 flexible, model-driven data management for experimental biology. Nat Methods. 2012;9(3):245-
644 53.

645 46. Liao Y, Smyth GK, Shi W. The R package Rsubread is easier, faster, cheaper and better
646 for alignment and quantification of RNA sequencing reads. Nucleic Acids Res. 2019;47(8):e47.

647 47. Chen Y, Lun AT, Smyth GK. From reads to genes to pathways: differential expression
648 analysis of RNA-Seq experiments using Rsubread and the edgeR quasi-likelihood pipeline.
649 F1000Res. 2016;5:1438.

650 48. Ritchie ME, Phipson B, Wu D, Hu Y, Law CW, Shi W, et al. limma powers differential
651 expression analyses for RNA-sequencing and microarray studies. Nucleic Acids Res.
652 2015;43(7):e47.

653 49. Robinson MD, Oshlack A. A scaling normalization method for differential expression
654 analysis of RNA-seq data. *Genome Biol.* 2010;11(3):R25.

655 50. Liu R, Holik AZ, Su S, Jansz N, Chen K, Leong HS, et al. Why weight? Modelling
656 sample and observational level variability improves power in RNA-seq analyses. *Nucleic Acids*
657 *Res.* 2015;43(15):e97.

658 51. Law CW, Chen Y, Shi W, Smyth GK. voom: Precision weights unlock linear model
659 analysis tools for RNA-seq read counts. *Genome Biol.* 2014;15(2):R29.

660 52. Phipson B, Lee S, Majewski IJ, Alexander WS, Smyth GK. Robust Hyperparameter
661 Estimation Protects against Hypervariable Genes and Improves Power to Detect Differential
662 Expression. *Ann Appl Stat.* 2016;10(2):946-63.

663 53. Smyth GK, Michaud J, Scott HS. Use of within-array replicate spots for assessing
664 differential expression in microarray experiments. *Bioinformatics.* 2005;21(9):2067-75.

665 54. Wu D, Lim E, Vaillant F, Asselin-Labat ML, Visvader JE, Smyth GK. ROAST: rotation
666 gene set tests for complex microarray experiments. *Bioinformatics.* 2010;26(17):2176-82.

667

668 **Figure Legends**

669

670 **Figure 1: Early thymic atrophy and T cell defects in *Hoil-1*^{ΔFoxn1} and *Hoip*^{ΔFoxn1} mice**

671 (A) RNA-seq expression analysis of LUBAC components from cTECs, mTEC^{hi} and mTEC^{low}
672 from 8-week-old WT mice. (B) Thymic cellularity of 8-week-old *Hoil-1*^{ΔFoxn1} or *Hoip*^{ΔFoxn1}, 6-
673 week-old *Sh^{cpdm/cpdm}*, mice versus controls. (C) Flow cytometry plots of thymocyte CD4 vs. CD8
674 expression from 8-week-old *Hoil-1*^{ΔFoxn1} mice and *Hoil-1*^{lox/lox} controls, with cell numbers
675 quantified (left panel). (D) Thymocyte subset numbers in 3-week-old *Hoip*^{lox/lox} and *Hoip*^{ΔFoxn1}
676 mice. (E) Numbers of splenic TCRβ⁺CD4⁺ and TCRβ⁺CD8⁺ T cells from 8-week-old *Hoil-*
677 *1*^{ΔFoxn1} and *Hoil-1*^{lox/lox} mice. (F) Flow cytometry plots of CD44 vs. CD62L expression gated on
678 splenic TCRβ⁺CD4⁺ or TCRβ⁺CD8⁺ T cells from 8-week-old *Hoil-1*^{ΔFoxn1} mice and *Hoil-1*^{lox/lox}
679 controls. Graphs show the numbers of naïve (CD44^{low}/CD62L^{high}), effector (CD44^{high}/CD62L^{low})
680 and central memory (CD44^{high}/CD62L^{high}) T cells. (G) Thymic cellularity of control and *Hoil-*
681 *1*^{ΔFoxn1} mice at the indicated ages. The numbers in parentheses indicate the mean fold-change in
682 thymic cellularity (controls vs *Hoil-1*^{ΔFoxn1} mice). All data are representative of at least two
683 independent experiments shown (except A) (n≥3/group). Graphs show mean ± SEM and groups
684 were compared with a Student's t test (two-sided, unpaired). * p<0.05, ** p<0.01; *** p<0.001;
685 **** p<0.0001.

686

687 **Figure 2: Loss of TECs and severe disruption of thymic architecture in *Hoil-1*^{ΔFoxn1} and**
688 ***Hoip*^{ΔFoxn1} mice.**

689 TEC (CD45⁻MHCII⁺EpCAM⁺) number from (A) 13-week-old *Hoil-1*^{lox/lox} and *Hoil-1*^{ΔFoxn1} mice
690 or (B) 13-week-old *Hoip*^{lox/lox} and *Hoip*^{ΔFoxn1} mice. Representative flow cytometry plots gated on
691 TECs from (C) 13-week-old *Hoil-1*^{lox/lox} and *Hoil-1*^{ΔFoxn1} mice or (D) 13-week-old *Hoip*^{lox/lox} and
692 *Hoip*^{ΔFoxn1} mice showing Ly51 vs. UEA-1 expression. (E, F) Mean proportion and number of
693 cTECs (Ly51⁺UEA-1⁻), mTECs (Ly51⁻UEA-1⁺) or “double negative” TECs (Ly51⁻UEA-1⁻) from
694 (E) 13-week-old *Hoil-1*^{lox/lox} and *Hoil-1*^{ΔFoxn1} mice or (F) 13-week-old *Hoip*^{lox/lox} and *Hoip*^{ΔFoxn1}
695 mice. (G-L) Immunofluorescence images of thymic sections from 8-9-week-old *Hoil-1*^{lox/lox},
696 *Hoil-1*^{ΔFoxn1}, *Hoip*^{lox/lox} and *Hoip*^{ΔFoxn1} mice stained with anti-K8 and UEA-1 (G, J), anti-K5 and
697 anti-AIRE (H, K) and ER-TR7 and anti-PanK (I, L). Scale bars represent 200 μm (G, I, J, L)
698 and 20 μm (H, K). * and ** represents epithelial-cell free regions. Data are representative of at
699 least two independent experiments (n ≥ 3/group). Graph bars indicate mean ± SEM and groups
700 were compared with a Student's t test (two sided, unpaired). * p<0.05; ** p<0.01; *** p<0.001;
701 **** p<0.0001.

702

703 **Figure 3: HOIL-1 deficiency induces early loss of mTECs in *Hoil-1^{ΔFoxn1}* mice.**

704 **(A)** TEC (CD45⁻MHCII⁺EpCAM⁺) numbers from E15.5 or 4-day-old *Hoil-1^{lox/lox}* and *Hoil-*

705 *^{ΔFoxn1}* mice. **(B)** Representative flow cytometry plots from thymic digests from individual E15.5

706 or 4-day-old *Hoil-1^{lox/lox}* and *Hoil-1^{ΔFoxn1}* mice showing Ly51 vs. UEA-1 gated on TECs (left and

707 middle panels) and CD80 vs. UEA-1 gated on mTECs (right panels). Graphs showing mean

708 proportions (top; of total TEC) and absolute numbers (bottom) of cTECs (Ly51⁺UEA-1⁻) and

709 total mTECs (Ly51⁻UEA-1⁺) from E15.5 **(C)** or cTECs, CD80^{hi} mTECs and CD80^{lo/-} mTECs

710 from 4-day-old **(D)** *Hoil-1^{lox/lox}* and *Hoil-1^{ΔFoxn1}* mice. **(E)** Representative flow cytometry plots of

711 MHC II vs AIRE expression gated on CD80^{hi} mTECs from 4-day-old *Hoil-1^{lox/lox}* and *Hoil-*

712 *^{ΔFoxn1}* mice and mean cell numbers. **(F)** Representative histograms and **(G)** graphs showing

713 proportions of proliferating Ki67⁺ TECs. **(H-J)** Immunofluorescence images of thymic sections

714 from 4-day-old *Hoil-1^{lox/lox}* and *Hoil-1^{ΔFoxn1}* mice stained with anti-K8 and UEA-1 **(H)**, anti-K5

715 and AIRE **(I)** and ER-TR7 and anti-PanK **(J)**. Scale bars represent 200 μm **(H, J)** and 20 μm **(I)**.

716 Graph bars indicate mean ± SEM and experiments with two groups were compared with a

717 Student's t test (two sided, unpaired)

718

719 **Figure 4: HOIL-1 is required to prevent TEC cell death**

720 **(A)** Multidimensional scaling (MDS) plot of RNAseq data from purified cTECs and mTEC^{hi}
721 from 2-week-old *Hoil-1^{lox/lox}* and *Hoil-1^{ΔFoxn1}* mice, taking into account the top 500 most variable
722 genes between a given two samples. **(B)** Plots of the log-fold changes (*Hoil-1^{ΔFoxn1}*/*Hoil-1^{lox/lox}*)
723 vs average expression for all genes in cTECs (top) and mTEC^{hi} (bottom). Those genes that are
724 significantly upregulated (red) or downregulated (blue) in cell subsets from *Hoil-1^{ΔFoxn1}* mice
725 when compared to *Hoil-1^{lox/lox}* control mice are highlighted. **(C)** Heatmaps showing the
726 expression of genes involved in necroptosis (GO:0070266) in purified mTEC^{hi} and cTEC
727 subsets. **(D)** Graph of the mean thymic cellularity in 8-week-old *Hoil-1^{ΔFoxn1} Casp8^{-/-} Mkl1^{-/-}* mice
728 vs controls. **(E)** Graph of the proportions of T cells among splenocytes in *Hoil-1^{ΔFoxn1} Casp8^{-/-}*
729 *Mkl1^{-/-}* mice vs controls. **(F-H)** Graph of the total number of TECs **(F)**, mTECs **(G)** or cTECs **(H)**
730 recovered from 8-week-old *Hoil-1^{ΔFoxn1} Casp8^{-/-} Mkl1^{-/-}* mice vs controls. Data are combined from
731 three independent experiments (n≥1-3/group). Graph bars indicate mean ± SEM. **(I, J)**
732 Immunofluorescence images of thymic sections from 8-week-old *Hoil-1^{lox/lox}* and *Hoil-*
733 *1^{ΔFoxn1} Casp8^{-/-} Mkl1^{-/-}* mice stained with anti-K8, anti-K5 and UEA-1 (scale bar = 200 μm).
734

735 **Figure 5: SHARPIN is required for mTEC^{lo}.**

736 (A) TEC (CD45⁻MHCII⁺EpCAM⁺) numbers from 6-week-old controls and *cpdm* mice. (B)
737 Representative flow cytometry plots and (C) graphs showing proportions and absolute numbers
738 of mTEC^{hi} (MHCII^{hi}Ly51⁻) and mTEC^{lo} mTECs (MHCII^{lo}Ly51⁻) and cTECs (MHCII⁺Ly51⁺).
739 Immunofluorescence images of thymic sections from 6-week-old *Sh^{cpdm/+}* and *Sh^{cpdm/cpdm}* mice
740 stained with (D) anti-K8 and UEA-1, (E) anti-K5 and AIRE and (F) ER-TR7 and anti-PanK.
741 Numbers of (G) TEC subsets in *Sh^{cpdm/cpdm}*, *Sh^{cpdm/cpdm} Casp8^{+/-} Ripk3^{-/-}*, *Sh^{cpdm/cpdm} Casp8^{-/-} Mkl1^{-/-}*,
742 (H) *Sh^{cpdm/+} Tnf^{-/-}*, *Sh^{cpdm/cpdm} Tnf^{-/-}*. Graph bars indicate mean ± SEM and groups were compared
743 with a Student's t test (two sided, unpaired). NS, not significant * p<0.05; ** p<0.01; ***
744 p<0.001; **** p<0.0001. The control group combines various combinations of genotypes (*Sh^{+/+}*,
745 *Sh^{cpdm/+}*; n≥ 3/group). Scale bars represent 100 μm (D, F) and 20 μm (E).

746

Figure 1

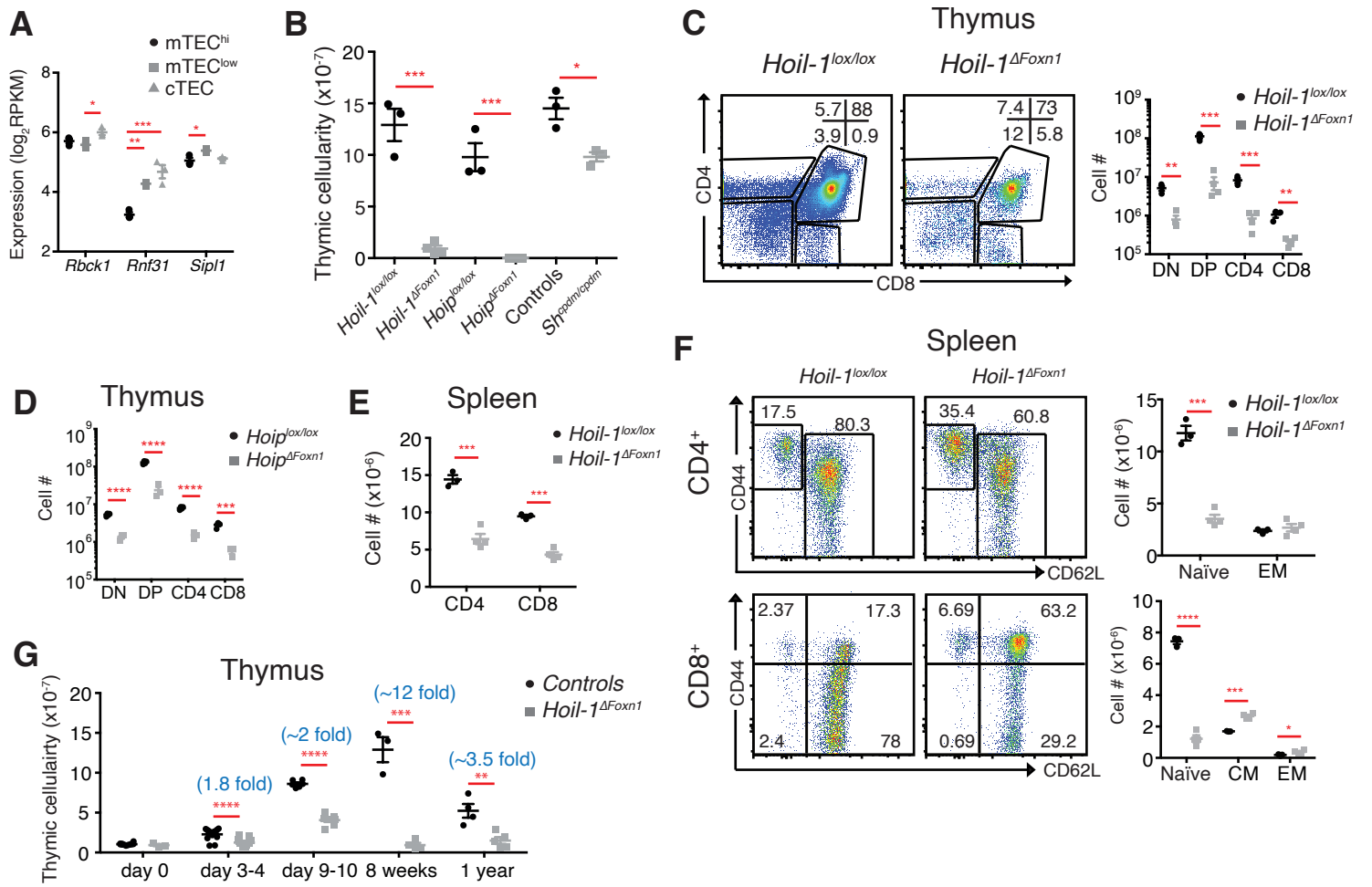


Figure 2

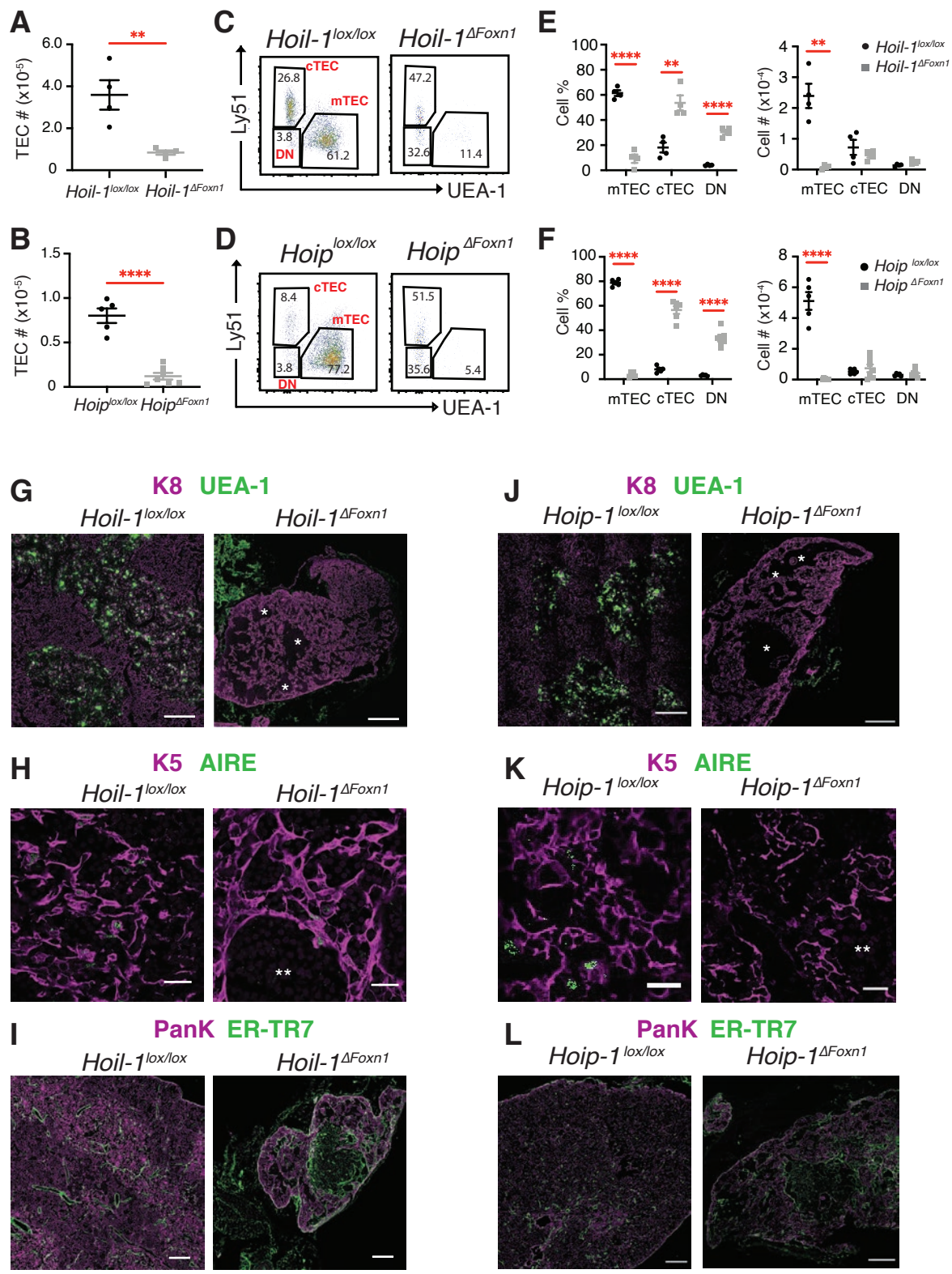


Figure 3

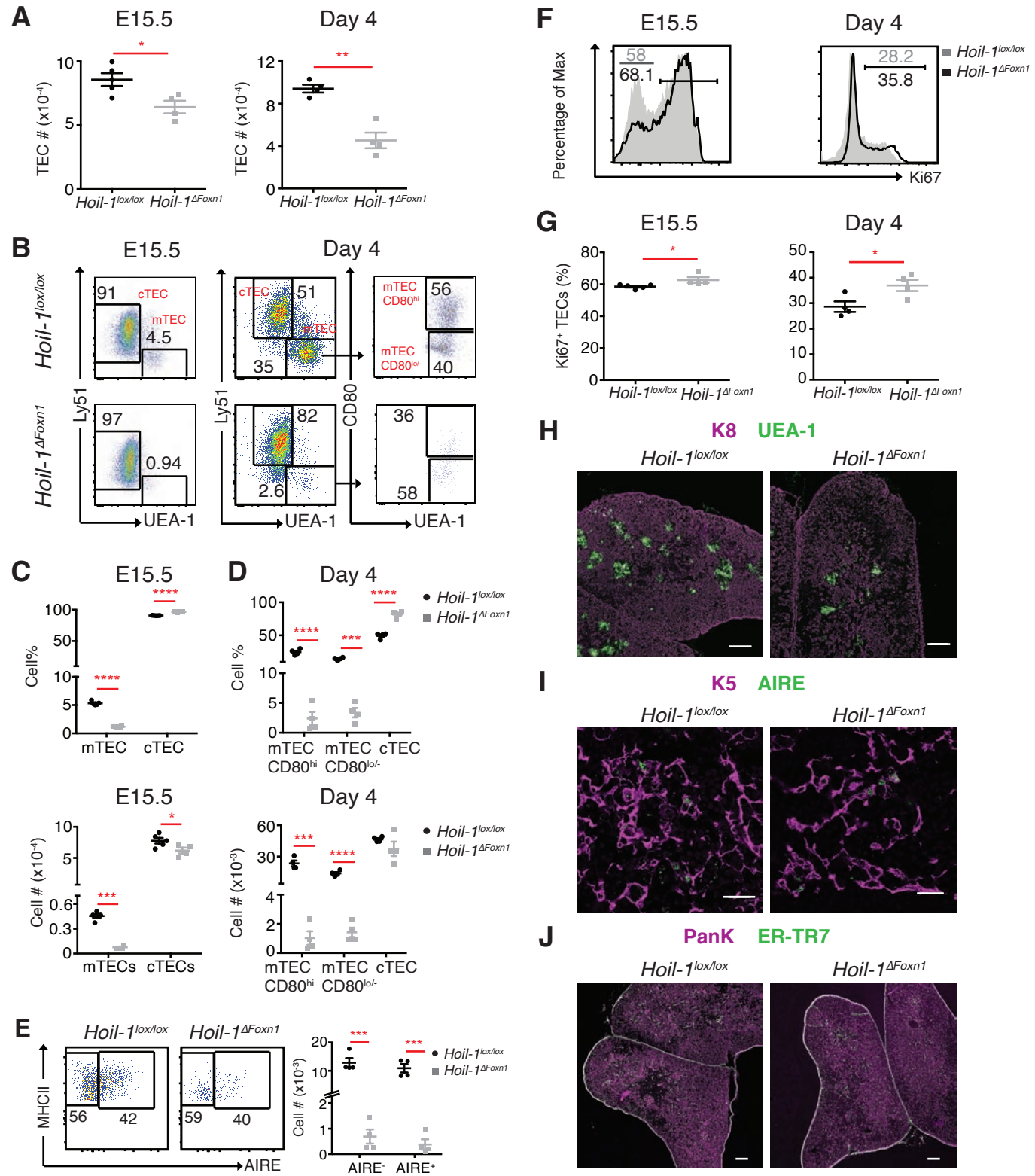


Figure 4

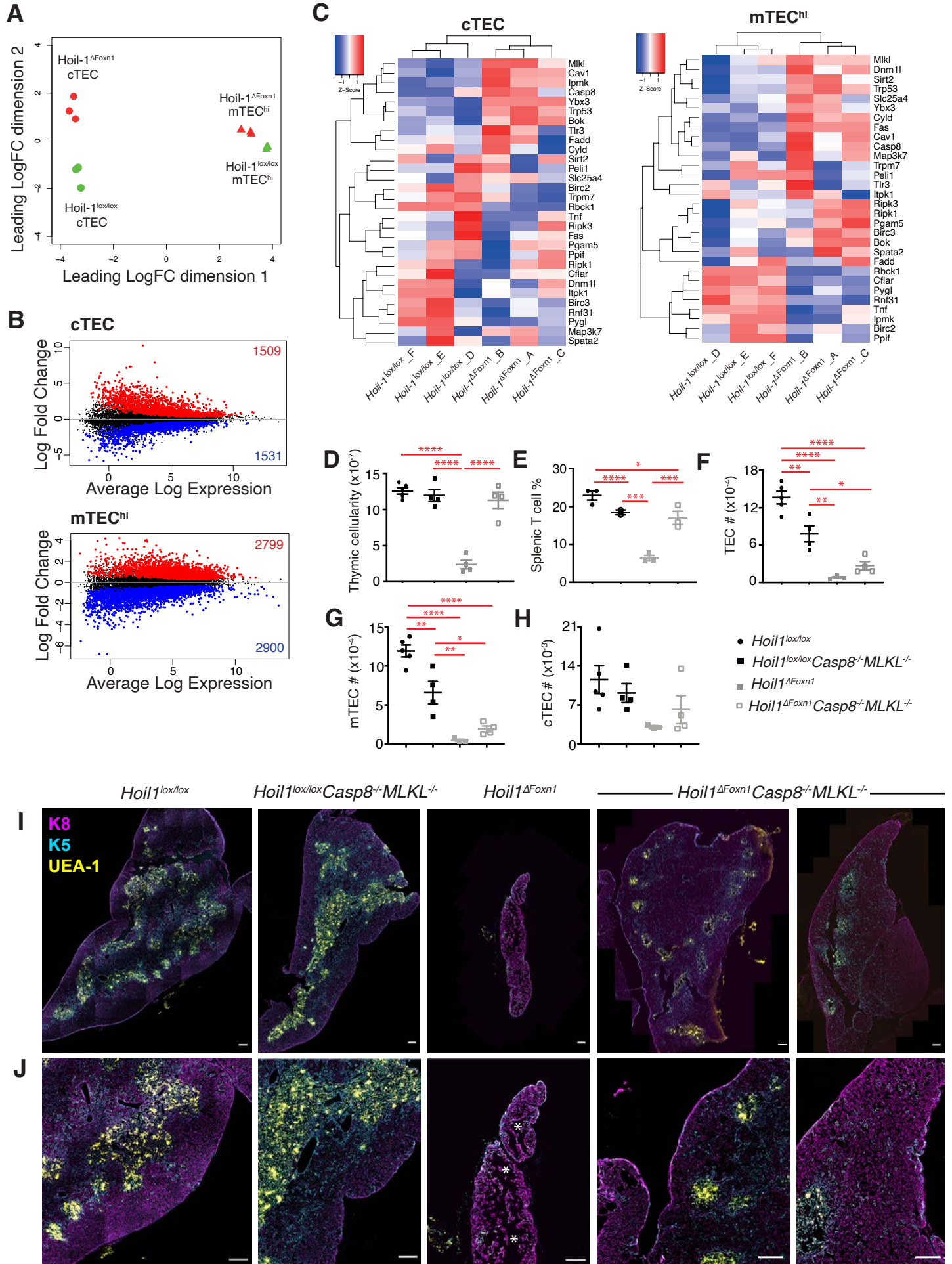


Figure 5

